Development of an Adaptive Artifact Subspace Reconstruction Based on Hebbian/Anti-Hebbian Learning Networks for Enhancing BCI Performance

Bo-Yu Tsai[®], Sandeep Vara Sankar Diddi[®], *Student Member, IEEE*, Li-Wei Ko[®], *Member, IEEE*, Shuu-Jiun Wang[®], Chi-Yuan Chang[®], *Student Member, IEEE*, and Tzyy-Ping Jung[®], *Fellow, IEEE*

Abstract—Brain—computer interface (BCI) actively translates the brain signals into executable actions by establishing direct communication between the human brain and external devices. Recording brain activity through electroencephalography (EEG) is generally contaminated with both physiological and nonphysiological artifacts, which significantly hinders the BCI performance. Artifact subspace reconstruction (ASR) is a well-known statistical technique that automatically removes artifact components by determining the rejection threshold based on the initial reference EEG segment in multichannel EEG recordings. In real-world applications, the fixed threshold may limit the efficacy of the

Manuscript received August 31, 2021; revised February 22, 2022; accepted April 27, 2022. This work was supported in part by the Ministry of Science and Technology (MOST) under Grant 108-2221-E-009-045-MY3, Grant 110-2321-B-010-005, and Grant 111-2321-B-A49-004 and in part by the Center for Intelligent Drug Systems and Smart Bio-Devices (IDS²B) from the Featured Areas Research Center Program within the framework of the Higher Education Sprout Project through the National Yang Ming Chiao Tung University (NYCU) and Ministry of Education (MOE) in Taiwan. (Bo-Yu Tsai and Sandeep Vara Sankar Diddi contributed equally to this work.) (Corresponding author: Li-Wei Ko.)

This work involved human subjects in its research. Approval of all ethical and experimental procedures and protocols was granted by the Research Ethics Committee (REC) of the National Yang Ming Chiao Tung University, Hsinchu, Taiwan, under Approval No. NCTU-REC-108-085E for performing the SSVEP BCI Experiment and Approval No. NCTU-REC-104-033 for performing the RSVP BCI Experiment.

Bo-Yu Tsai is with the Institute of Biomedical Engineering and the Brain Research Center, National Yang Ming Chiao Tung University, Hsinchu 300, Taiwan.

Sandeep Vara Sankar Diddi is with the International Ph.D. Program in Interdisciplinary Neuroscience and the Center for Intelligent Drug Systems and Smart Bio-devices (IDS2B), National Yang Ming Chiao Tung University, Hsinchu 300. Taiwan.

Li-Wei Ko is with the Institute of Bioinformatics and Systems Biology, International Ph.D. Program in Interdisciplinary Neuroscience, and the Center for Intelligent Drug Systems and Smart Bio-devices (IDS2B), College of Biological Science and Technology, National Yang Ming Chiao Tung University, Hsinchu 300, Taiwan, also with the Department of Electronics and Electrical Engineering, the Institute of Electrical and Control Engineering and the Institute of Biomedical Engineering, and the Brain Research Center, College of Electrical and Computer Engineering, National Yang Ming Chiao Tung University, Hsinchu 300, Taiwan, and also with the Department of Biomedical Science and Environment Biology and the Drug Development and Value Creation Research Center, Kaohsiung Medical University, Kaohsiung 807, Taiwan (e-mail: lwko@nycu.edu.tw).

Shuu-Jiun Wang is with the Taipei Veterans General Hospital, Taipei 11217, Taiwan, and also with the Brain Research Center and the School of Medicine, National Yang Ming Chiao Tung University, Taipei 112, Taiwan.

Chi-Yuan Chang and Tzyy-Ping Jung are with the Swartz Center for Computational Neuroscience, University of California, San Diego, San Diego, CA 92093 USA.

Color versions of one or more figures in this article are available at https://doi.org/10.1109/TNNLS.2022.3174528.

Digital Object Identifier 10.1109/TNNLS.2022.3174528

artifact correction, especially when the quality of the reference data is poor. This study proposes an adaptive online ASR technique by integrating the Hebbian/anti-Hebbian neural networks into the ASR algorithm, namely, principle subspace projection ASR (PSP-ASR) and principal subspace whitening ASR (PSW-ASR) that segmentwise self-organize the artifact subspace by updating the synaptic weights according to the Hebbian and anti-Hebbian learning rules. The effectiveness of the proposed algorithm is compared to the conventional ASR approaches on benchmark EEG dataset and three BCI frameworks, including steady-state visual evoked potential (SSVEP), rapid serial visual presentation (RSVP), and motor imagery (MI) by evaluating the root-mean-square error (RMSE), the signal-to-noise ratio (SNR), the Pearson correlation, and classification accuracy. The results demonstrated that the PSW-ASR algorithm effectively removed the EEG artifacts and retained the activity-specific brain signals compared to the PSP-ASR, standard ASR (Init-ASR), and moving-window ASR (MW-ASR) methods, thereby enhancing the SSVEP, RSVP, and MI BCI performances. Finally, our empirical results from the PSW-ASR algorithm suggested the choice of an aggressive cutoff range of c = 1-10 for activity-specific BCI applications and a moderate range of c > 10 for the benchmark dataset and general BCI applications.

Index Terms—Artifact removal, artifact subspace reconstruction, brain-computer interface (BCI), electroencephalography, Hebbian/anti-Hebbian neural network.

I. INTRODUCTION

RAIN-COMPUTER Interface (BCI) translates the indi-Byidual's desire to execute a variety of user-specific interactions by establishing a direct connection between the user's brain and an external device [1], [2]. BCI is proven to be a potential tool that can largely benefit the neurologically affected patients by assisting their needs and improving the quality of life [3]. Electroencephalography (EEG) is one of the most widely used signal acquisition tools in the field of cognitive neuroscience. Although many modalities, such as functional magnetic resonance imaging (fMRI) and positron emission tomography (PET), are available, EEG attains popularity because of its high time resolution, portability, and reliability [4]. EEG records the electrical activity of the brain through electrodes placed on the scalp. During the acquisition process, EEG signals are known to be contaminated by unwanted noises resulting from various artifacts affecting the BCI performance. These artifacts may be caused by measuring equipment, external environments, or power-line noise, which

2162-237X © 2022 IEEE. Personal use is permitted, but republication/redistribution requires IEEE permission. See https://www.ieee.org/publications/rights/index.html for more information.

are nonphysiological in nature and can be eliminated by choosing the right recording instruments, acquisition mechanism, and filtering techniques. Voluntary and involuntary activities, such as eye movements, eye blinking, heart sounds, and muscle activities, cause physiological artifacts that interfere with the brain signals and mislead the understanding of the neural activity, especially in BCI applications [5]–[9]. Thus, in order to improve the BCI performance, the removal of these physiological and nonphysiological artifacts before the EEG signal analysis is inevitable. In addition, the choice of an EEG acquisition system that is compatible with real-world applications is crucial. [10], [11] suggested wearable and wireless EEG devices are relatively comfortable, quick to set up, easy to use, mobile, and offer acceptable signal quality compared to wired EEG systems.

The literature shows the increased focus on developing various artifact removal techniques to eliminate nonbrain components from the recorded EEG signals. Blind source separation (BSS) [12], [13] is a conventional method that works on the principle of signal source separation. BSS decomposes the original contaminated signal into clean and artifact components. However, the quality of the signal separation depends on the types and degrees of contamination. The independent component analysis (ICA) [14], [15] and the principal component analysis (PCA) [16] are the most commonly preferred BSS techniques to handle source separation problems and in removing the artifact components from the EEG data. Regression [17]-[19] methods are also applied to remove artifacts in EEG signals but only limited to off-line processing due to their dependency on the reference [electrooculogram (EOG), electrocardiogram (ECG), or electromyogram (EMG)] to remove corresponding components from the EEG records. Empirical mode decomposition (EMD) [20], [21] uses intrinsic mode functions (IMFs) to recursively decompose the EEG signals into modes and remove unwanted amplitude- and frequency-modulated (AM/FM) components, but it is very sensitive to noise and restricted only to off-line processing.

An automatic artifact removal technique with online compatibility is extremely important to handle real-time BCI processing. [22] proposed an automatic and online-capable artifact subspace reconstruction (ASR), which is a PCA-statistic method for removing large-amplitude artifacts. Furthermore, EEGLAB [23], which is an open-source MATLAB package proposed by the Swartz center for computational neuroscience (SCCN), offers the basic ASR implementation. [24], [25] further analyzed ASR to validate its effectiveness and the strictness of a cutoff parameter on real EEG data. An automatic IC classifier (ICLabel) is used to identify brain and artifact components to quantitatively and objectively assess the ASR's effectiveness in removing artifacts and preserving brain activities. [26] discussed the artifact-reduction specificity on visual evoked potentials (VEP) by replacing the traditional Euclidean geometry used in the ASR method with the Riemannian geometry to handle the curved and high-dimensional data space covariance matrices. According to the ASR implementation, the artifact subspace of the reference data is fixed for reconstructing the entire EEG data, which may hinder the performance of artifact

removal, especially during real-time applications with initial large-amplitude artifacts. In general, the artifact subspace of the reference data should be adaptive and able to underlie the mechanics of the whole EEG dataset [27]–[29].

Hebbian and anti-Hebbian networks are potential selforganizable single-layered learning networks in which Hebbian rules align the synaptic weight feature vectors with the input space direction of greatest variance, while anti-Hebbian rule mediates and prevents the feature vectors from aligning in the same direction [30], [31]. However, the Hebbian and anti-Hebbian learning rules optimized on a full network lead to biologically implausible nonlocal learning rules where synaptic weights depend on the neural activities rather than the neural connections. This problem can be mitigated by reducing the optimization problem to the synaptic level, thereby solving locally to achieve biological plausibility. Recently, a Hebbian/anti-Hebbian learning network with a multidimensional scaling cost function method using local learning rules was proposed to solve the subspace-tracking problem [32], which guarantees convergence to a unique fixed-point with the min-max optimization theorem. This optimization technique allows one to derive the biologically plausible local learning rules for both feedforward and lateral synaptic connections in Hebbian and anti-Hebbian networks, which obeys the potential relation between lateral synaptic and feedforward weights [33]. The Hebbian/anti-Hebbian networks derived from the classical multidimensional scale (CMDS) cost function are called principal subspace projection (PSP), and adding regularization to the PSP gives principle subspace whitening (PSW) [30], [34]. Both the PSP and PSW algorithms applied on the basis of local learning rules produce significant performance improvements during off-line and online analyses compared to Oja's network [35] and general Hebbian algorithm [36] for subspace tracking in the singlelayer networks.

This study aims to develop an online capable adaptive ASR algorithm to remove artifact components effectively and enhance the BCI performance. The adaptive ASR algorithm self-organizes the artifact subspace by applying the Hebbian/anti-Hebbian learning networks for every small segment of the streaming EEG data. The Hebbian/anti-Hebbian learning network integrated into the ASR algorithm updates the mixing matrix and threshold values by learning the dynamics of the streaming EEG data segment through biologically plausible local learning rules, thereby eliminating the problem of picking either fixed or noisy artifact subspace. This study applied the proposed adaptive ASR algorithm on: 1) a benchmark dataset with clean EEG data contaminated by recorded EOG and simulated EMG signals; 2) steady-state visual evoked potential (SSVEP) BCI framework; 3) rapid serial visual presentation (RSVP) BCI framework; and 4) motor imagery (MI) BCI framework to evaluate the artifact correction performance. The results showed that the proposed adaptive ASR algorithms, particularly PSW-ASR, efficiently suppressed the artifactual components and improved the performance compared to the standard online ASR (Init-ASR) and moving-window ASR (MW-ASR) algorithms in all the experimental conditions. Furthermore, this study also discussed the

role of the cutoff parameter in determining the quality of the EEG reconstruction and their range for improved BCI performance. The demo code of the Adaptive ASR algorithm is available at https://github.com/t5i0m7/AASR.

The rest of the article is organized as follows. Section II presents the algorithms for conventional ASR and the proposed adaptive ASR techniques. Section III describes the experimental datasets, data preparation, and metrics evaluation to assess the performance. Section IV presents the performance comparison between the proposed and conventional algorithms for both the benchmark and three BCI frameworks. Section V discusses the uniqueness and potential of the adaptive ASR algorithm and the influence of the cutoff parameter on artifact removal. Finally, Section VI concludes this article with future scope.

II. ADAPTIVE ARTIFACT SUBSPACE RECONSTRUCTION

This section briefly describes the initial state online capable ASR algorithm (Init-ASR) and its functional scope followed by the implementation of moving-window-based ASR. Furthermore, Hebbian/anti-Hebbian neural network models are introduced for adaptive subspace tracking and its inclusion in the ASR architecture for efficient subspace tracking mechanism.

A. Artifact Subspace Reconstruction With Initial State

ASR is a statistical technique that automatically analyzes the EEG signals for artifacts by using a variance component. The algorithm rejects the large-variance components by comparing them with the clean EEG data components. In particular, the algorithm automatically identifies the clean EEG portion of the raw data as reference and learns its distribution to determine the constraint for rejecting artifactual components [24], [37]. During real-time EEG scenarios, it is not always possible to collect the entire EEG dataset and obtain a clean EEG segment. Instead, recording short initial segments of artifact-free EEG data as a reference is preferred to calculate artifact subspace. This reference subspace rejects the artifactual components of the incoming data and processes channelwise reconstruction from the remaining components [38]. This standard online ASR model is named Init-ASR in this study. For clear implementation details of the ASR algorithm, refer to [24].

Step 1: ASR automatically selects the clean EEG segments based on the signal variance distribution. In particular, the algorithm calculates the channelwise root-mean-square (rms) values for every 1-s window segment and uses truncated Gaussian distribution to calculate z-score for all those windowed rms values. The data with the z-scores range within -3.5 and 5.5 are concatenated to obtain reference data $D_r \in \mathbb{R}^{C \times L'}$, where C is the number of channels and L' is the data length of reference data. These reference data are used to calibrate ASR, and the data length depends on the amount of contamination.

Step 2: The chosen data D_r are passed through an IIR-filter to suppress specific frequency-band activities typically related to oscillatory activities in the brain, producing $\widetilde{D_r}$. This implies that the IIR-filter designed using the Yule-Walker method

suppresses the brain activity components and alleviates the artifact components, which are further analyzed to extract the artifact subspace. To calculate the projection of artifact subspace, ASR computes mixing matrix $M_r \in \mathbb{R}^{C \times C}$, which is the square root of $\text{Cov}(\widetilde{D_r})$ followed by eigenvalue decomposition to obtain eigenvectors $V_r \in \mathbb{R}^{C \times C}$ and eigenvalues λ_r . Using these eigenvectors V_r , each principal component $\widetilde{Y}_r \in \mathbb{R}^{C \times L'}$ can be calculated by projecting V_r on $\widetilde{D_r}$

$$\widetilde{Y}_r = V_r^T \widetilde{D}_r. \tag{1}$$

Furthermore, ASR calculates the mean (μ_i) and standard deviation (σ_i) of rms values for each component of \widetilde{Y}_r across all 0.5-s segments and calculates the rejection threshold for each component as

$$T_i = \mu_i + c\sigma_i \tag{2}$$

where c is the user-defined cutoff parameter and i represents the componentwise analysis.

Step 3: The unclean streaming data $D_t \in \mathbb{R}^{C \times L''}$, where L'' is the data length of streaming data, are initially preprocessed by IIR filter and extract covariance matrix to evaluate eigenvalue decomposition and obtain eigenvectors V_t and eigenvalues λ_t . To identify which components should be rejected, each principal component with variance λ_t is compared with the threshold T_i projected from V_r onto V_t

$$(\lambda_t)_j \ge \sum_i \left(T_i((V_r)_i)^T (V_t)_j \right)^2. \tag{3}$$

If the inequality holds, the corresponding components are replaced with the zero vectors called V'_t . With the initial assumption of ASR, we can get the clean latent components $(Z_t)_{\text{clean}}$ from the original latent variable $Z_t \in \mathbb{R}^{C \times L''}$

$$(Z_t)_{\text{clean}} = \left(\left(V_t' \right)^T M_r \right)^+ V_t^T D_t \tag{4}$$

where $(.)^+$ represents the pseudoinverse of (.).

Finally, the clean streaming data $(D_t)_{\text{clean}} \in \mathbb{R}^{D \times L''}$ are obtained by multiplying the mixing matrix M_r with $(Z_t)_{\text{clean}}$

$$(D_t)_{\text{clean}} = M_r(Z_t)_{\text{clean}} = M_r \left(\left(V_t' \right)^T M_r \right)^+ V_t^T D_t.$$
 (5)

B. Moving-Window Artifact Subspace Reconstruction

The choice of reference data limited to the initial recordings of the EEG signal might hinder the efficacy of the EEG artifact removal, especially when the reference data contain artifactual components or due to the dynamic nature of EEG activity over time such that the fixed threshold may not be reliable to reject artifacts and reconstruct the clean EEG data. An alternate way is to update the threshold by calculating the artifact subspace for every sliding windowed segment. Thus, an online ASR algorithm by recalculating artifact subspace using windowed segments called moving window artifact subspace reconstruction (MW-ASR) is used. The artifact subspace is evaluated and updated for every 20-s window.

C. Hebbian/Anti-Hebbian Network for Subspace Tracking

Simply applying MW-ASR without a continuous parameter updation mechanism may not serve the purpose of efficient

artifact removal, and moreover, reducing the dimensionality of streaming data during the data analysis process is very important. Hebbian and anti-Hebbian rules are the biologically plausible single-layer neural networks that self-organize through local learning rules and help in reducing the dimension of the networks [34]. The Hebbian and anti-Hebbian learning rules compensate for the input space feature vectors' directions to the optimum variance that results in equilibrium where the feedforward and lateral synaptic weight vectors span the principal subspace of the input covariance matrix. Pehlvan et al. [32] proposed an online similarity matching algorithm using a multidimensional scaling objective function to determine the similarity matching of the principal subspace projection (PSP) through local learning rules and describe the result of the batch optimization for the multidimensional scaling cost function leading to Hebbian/anti-Hebbian learning networks. The batch optimization function for quantifying the similarity can be written by (6), where $X_k \in \mathbb{R}^{C \times N}$ is the batch input data obtained after the IIR filtering and $Y_k \in \mathbb{R}^{C \times N}$ is the batch subspace data obtained by the projection onto the principal subspace corresponding to the input covariance matrix, C determines the number of channels, k is the kth element in the batch segment, and N is the number of batch segments

$$\min_{Y_k} \sum_{k=1}^{N} || (X_k^T X_k - Y_k^T Y_k) ||_F^2.$$
 (6)

To optimize Y_k , the covariance matrices $1/nX_kX_k^T$ and $1/nY_kY_k^T$ are replaced with the dynamic variable matrices $W \in$ $\mathbb{R}^{C \times C}$ and $M \in \mathbb{R}^{C \times C}$, where W is the feedforward synaptic weight matrix and M is the lateral synaptic weight matrix, and derive the min-max PSP objective by modifying (6) as follows:

$$\min_{Y_k} \min_{W} \max_{M} \ 2Tr(W^T W) - Tr(M^T M)$$

$$-4\sum_{k=1}^{N}X_{k}^{T}W^{T}Y_{k}+2\sum_{k=1}^{N}Y_{k}^{T}M^{T}Y_{k}.$$
 (7)

The positive definite nature of M guarantees the function $-4\sum_{k=1}^{N}X_{k}^{T}W^{T}Y_{k}+2\sum_{k=1}^{N}Y_{k}^{T}M^{T}Y_{k}$ to converge to a unique fixed point $M^{-1}W^TX_k$. Finally, (7) can be further optimized by exchanging the order of minimization with respect to Y and W, and Y and maximization of M using the saddle point property which gives the following min-max optimization problem:

$$\min_{W} \max_{M} 2Tr(W^{T}W) - Tr(M^{T}M) - 2\sum_{k=1}^{N} X_{k}^{T}W^{T}Y_{k}$$
where $Y_{k} \equiv M^{-1}W^{T}X_{k}$. (8)

Using gradient descent-ascent updates with stochasticity for optimizing W and M in (8) deduces Algorithm 1, where the row vectors of $M^{-1}W$ are the projection of principal subspace when W and M converge. Algorithm 1 describes the whole optimization process using the Hebbian/anti-Hebbian learning network. The parameters r_W and r_M are the time-varying learning rates for Hebbian and anti-Hebbian neurons corresponding

Algorithm 1 Online PSP

Require: Initial neural weights for $W \in \mathbb{R}^{C \times C}$ and $M \in \mathbb{R}^{C \times C}$ $\mathbb{R}^{C \times C}$, where C represents number of channels

1: **for** k = 1:N **do**

2: $Y_k \Leftarrow M^{-1} W X_k$ 3: $W \Leftarrow (1 - r_W)W + r_W Y_k X_k^T$ 4: $M \Leftarrow (1 - r_M)M + r_M Y_k Y_k^T$

5: end for

Algorithm 2 Online PSW

Require: Initial neural weights for $W \in \mathbb{R}^{C \times C}$ and $M \in \mathbb{R}^{C \times C}$ $\mathbb{R}^{C \times C}$, where C represents the number of channels

1: for k = 1:N do

2: $Y_k \Leftarrow M^{-1} W X_k$ 3: $W \Leftarrow (1 - r'_W)W + r'_W Y_k X_k^T$ 4: $M \Leftarrow (M - r'_M I_k) + r'_M Y_k Y_k^T$

to W and M respectively, where $r_W = 2\eta$, η is the W learning rate in the range $0 < \eta/2 < 1$ and $r_M = r_W/2\tau$, and τ is the ratio of W and M learning rates with $\tau > 0$.

In addition, the authors extended the online similarity matching PSP algorithm by adding a constraint that spheres the principal subspace of the objective function resulting a whitening mechanism called principal subspace whitening (PSW). In the PSW network model, the data in the principal subspace is sphered such that the objective function attains unit variance across all the directions

$$\min_{Y_k} \sum_{k=1}^{N} || (X_k^T X_k - Y_k^T Y_k) ||_F^2 \quad \text{s.t.} \quad \frac{1}{S} Y_k Y_k^T = I$$
 (9)

where S is the length of the data in batch segment k.

Similar to the optimization methods in the PSP objective function, we can also derive the min-max PSW objective function using (10). Algorithm 2 shows the whole optimization process by applying gradient descent-ascent updates for W and M using the Hebbian/anti-Hebbian learning networks. The parameters r'_W and r'_M are the time varying-learning rates with constraint for Hebbian and anti-Hebbian neurons corresponding to W and M respectively, where $r'_W = \eta'$, η' is the W learning rate in the range $0 < \eta' < 1$ and $r'_M = r'_W/\tau'$, and τ' is the ratio of W and M learning rates with $\tau' > 0$

$$\min_{W} \max_{M} 2Tr(W^{T}W) - Tr(M) - 2\sum_{k=1}^{N} X_{k}^{T}W^{T}Y_{k}$$
where $Y_{k} \equiv M^{-1}W^{T}X_{k}$. (10)

D. Artifact Subspace Reconstruction With Hebbian/Anti-Hebbian Network

The ASR algorithm [24] states that it is necessary to record a segment reference data to evaluate mixing matrix M_r and set an artifact subspace threshold. However, the quality of the reference data plays a vital role when using the ASR algorithm

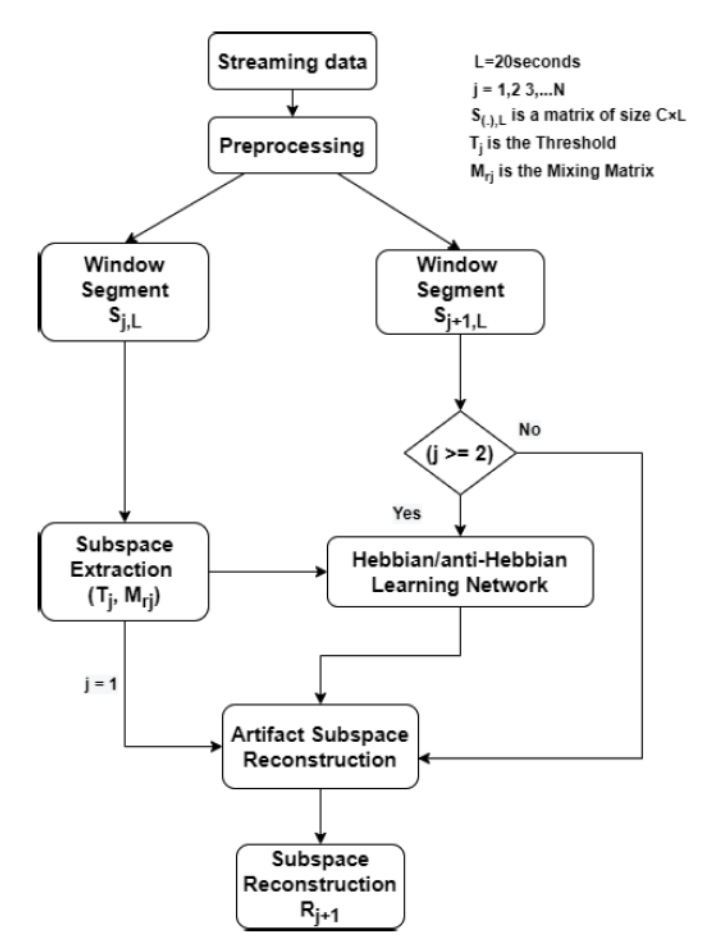


Fig. 1. Flowchart of the proposed PSP/PSW-ASR algorithm.

in a real-world scenario. It is possible to get a bad reference if the recordings have large voltage artifacts. Thus, the addition of the Hebbian/anti-Hebbian neural networks into the ASR algorithm to update the artifact subspace segmentwise helps the algorithm adapt to the streaming EEG data dynamics. The Hebbian/anti-Hebbian network updates the mixing matrix and threshold of artifact subspace for each data segment by applying local learning rules. The flowchart in Fig. 1 illustrates the whole flow of Hebbian/anti-Hebbian learning with ASR, which produces PSP-ASR and PSW-ASR. For every jth segment (j > 1), the mixing matrix (M_{rj}) and the threshold value (T_i) are updated using Hebbian/anti-Hebbian learning mechanism. By self-organizing the learnable synaptic weight neurons W and M with the data segment S_{i+1} using Algorithm 1 or Algorithm 2, we can reconstruct the data in the data segment S_{j+1} to R_{j+1} .

III. EXPERIMENTAL SETUP

The fundamental principle of the ASR algorithm is to remove artifact components based on the variance of component activities. However, the choice of the cutoff parameter (c) plays an important role in removing the unwanted artifacts and in preserving the brain activity components [24]. In this study, we applied Hebbian/anti-Hebbian neural networks to reconstruct artifact subspace for different ranges of c values and observe its effectiveness on the BCI performance compared to other conventional ASR methods. The performance of the

existing and proposed ASR algorithms was evaluated on four different BCI datasets. Fig. 2 illustrates the overall flow of our proposed analysis on: 1) Benchmark dataset and 2) SSVEP, RSVP, and MI BCI frameworks. All the experimental datasets were initially preprocessed to remove high-frequency and line noise components, and extract frequencies of interest using an FIR bandpass filter (BPF).

A. Benchmark Dataset

1) Experiment: Klados et al. [39] proposed a standard procedure for simulating EEG dataset with EOG artifacts. Twenty-seven subjects (14 males and 13 females) took part in the study, and each subject performed the experiment for one trial having 30-s duration. The semisimulated EEG data contain a combination of artifact-free EEG data recorded during an eyes-closed session and EOG data recorded during an eyes-opened session by applying the contamination model proposed in [39]. The artifact-free clean EEG data are recorded using a 19-channel EEG system placed according to the International 10-20 Standard. The EOG data are recorded using four electrodes with two electrodes placed above and below the left eye and the other two on the outer canthi of each eye resulting in two bipolar signals, namely, horizontal EOG (HEOG) and vertical EOG (VEOG). A linear regression analysis is performed to select the amplitude levels of HEOG and VEOG, and project them onto the clean EEG data during the contamination process to prepare EEG/EOG dataset. Furthermore, the trials with a close resemblance between clean EEG and contaminated EEG data are manually observed and removed from our analysis resulting data from 18 subjects for the study. Since the size of the data is too small, the contamination process is repeated six times by projecting the HEOG and VEOG onto the clean EEG data producing six trials of the EEG/EOG dataset for each subject.

In addition to EOG contamination, we also investigated the influence of muscle artifacts on the EEG signal by simulating the EMG signal using the EMG simulator toolbox proposed by [40]. A projection matrix is designed to map the EMG artifacts onto the temporal regions of the brain to prepare the EEG/EMG dataset [41]. The contamination process is repeated six times by projecting the EMG artifacts producing six trials for each subject. The toolbox ensures that the simulated EMG signals derived by the design function and projected onto the EEG signals are similar to the clinically recorded muscle artifact EEG signals [42].

2) Data Preparation and Metrics: The 30-s duration of each trial is chopped into a 24-s data segment between 4 and 27 s to eliminate any uncertainty caused during the start and end duration of the experiment. Then, two consecutive trials of the EOG/EMG contaminated EEG signals were stacked to form three 48-s segment datasets, respectively, for each subject. Furthermore, a clean EEG signal is chopped similarly for 24 s and repetitively stacked twice to form two 48-s segment datasets. Finally, the 48-s segments of the contaminated (A) and clean (C) EEG signals are concatenated, as shown in Fig. 3, to produce a 240-s data segment. Since our proposed Hebbian/anti-Hebbian learning ASR algorithm is designed to calculate artifact subspace for every 20-s duration, this

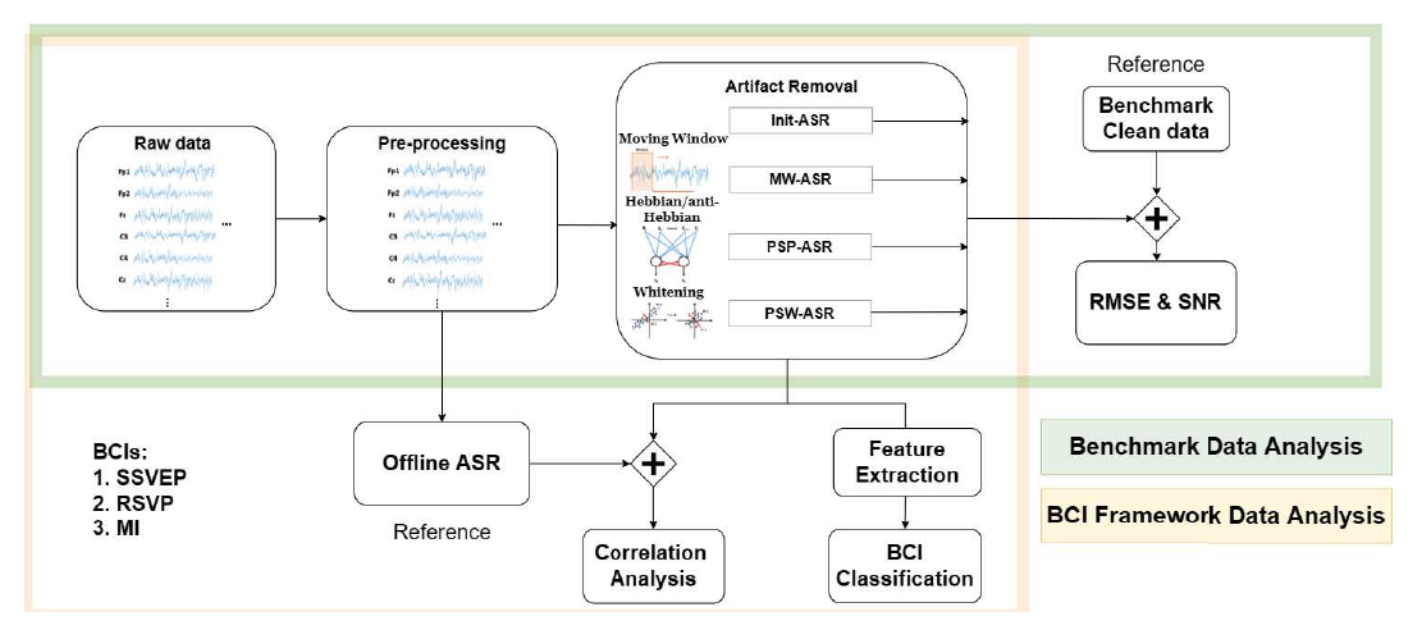


Fig. 2. Block representation of the BCI system framework with artifact removal mechanism using proposed and existing online ASR algorithms. The analysis of the benchmark dataset is highlighted by the green box and the BCI framework by the orange box.

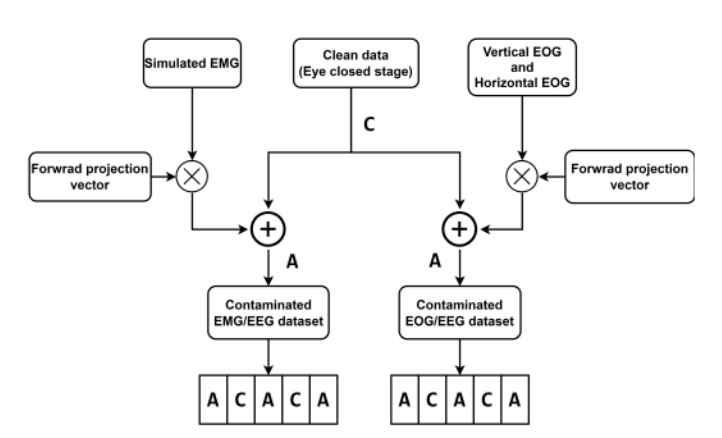


Fig. 3. Flow diagram of EOG/EMG contaminated EEG dataset. A and C represent contaminated and clean EEG signals.

concatenation mechanism allows the algorithm to self-adjust to the signal distribution of clean and contaminated signals. The projection vectors of EOG and EMG datasets were designed, as proposed by [39], [40].

To evaluate the performance of each algorithm, the root mean square error (RMSE) and signal-to-noise ratio (SNR) metrics were analyzed. RMSE is a Euclidean distance metric to measure the difference between the estimator and the observed values (11), while SNR measures the ratio of desired signal power to the background noise power 12)

RMSE =
$$\sqrt{\frac{\sum_{t=1}^{n} (X_t - Y_t)^2}{n}}$$
 (11)
SNR_{dB} = $10 \log_{10} \frac{\sum_{t=1}^{n} X_t^2}{\sum_{t=1}^{n} N_t^2}$ (12)

$$SNR_{dB} = 10 \log_{10} \frac{\sum_{t=1}^{n} X_{t}^{2}}{\sum_{t=1}^{n} N_{t}^{2}}$$
 (12)

where X_t is the processed EEG signal after artifact removal, Y_t is the clean EEG signal, N_t is the noise (EOG/EMG) signal, nis the number of sample points, and dB is decibels. The RMSE and SNR are calculated for each subject across the channels.

B. SSVEP BCI Framework

1) Experiment and Data Preparation: SSVEPs are the natural responses elicited by the flickering visual stimuli flashed at specific frequencies [2], [43]. The SSVEP BCI experiment is a simulated military shooting scenario proposed by Ko et al. [44], where three soldiers appear on the screen with a flickering icon in front of each soldier as a target, which are flickered at their predefined frequencies (8, 9, and 14 Hz). The system picks the target from the experimental subject's EEG response, which depends on the presented stimulus frequency and then shoots the derived target. Fifteen subjects participated in the study aged between 18 and 26 years, and this study was performed in accordance with the recommendations of the Institutional Review Board of National Yang Ming Chiao Tung University, Hsinchu, Taiwan, and was approved by the Research Ethics Committee of National Yang Ming Chiao Tung University, Hsinchu, Taiwan, under the protocol code NCTU-REC-108-085E. Each experiment consists of 30 trials with each trial having three stages, namely, fixation, searching, and stimulus stages. Each trial lasts for a 13-s duration containing 2-s fixation, 5-s target search, and 6-s visual stimuli. During the experiment, all the subjects had normal eye-blinking, eye movement, and muscle activities, which contaminated the EEG signals. A 1-50-Hz BPF is applied to the EEG signal to remove high frequency and line noise. Finally, all the trials are concatenated subjectwise to ensure sufficient eye and muscle artifacts in the EEG recordings for further analysis.

2) Pearson Correlation: The performance of the reconstructed EEG signal after the artifact correction mechanism with reference to the ground-truth EEG data is evaluated using correlation analysis. Correlation is a statistical measure of evaluating the strength of the relationship between two EEG signals, X and Y. Specifically, the Pearson correlation coefficient (ρ) is computed to examine the significance of similarity by using the following:

$$\rho = \frac{\sum_{t=1}^{n} (X_t - \bar{X})(Y_t - \bar{Y})}{\sqrt{\sum_{t=1}^{n} (X_t - \bar{X})^2} \sqrt{\sum_{t=1}^{n} (Y_t - \bar{Y})^2}}$$
(13)

where \bar{X} and \bar{Y} are the mean values of X and Y, and n represents number of sample points.

3) Accuracy: Accuracy measures the degree of exactness with reference to the actual value. To improve the BCI performance, differential power (DP) proposed by [45] is calculated to extract the features of each SSVEP frequency by choosing the dominant target frequency power, i.e., DP measures the ratio of target frequency power to the mean of the nontarget frequency powers, as follows:

$$DP(f_T) = \frac{P(f_T)}{\frac{1}{N-1} \left(\sum_{k=1}^{N} P(f_k) - p(f_T) \right)}$$
(14)

where P(.) determines the signal power, f_T is the target frequency, and N is the total target frequency components.

C. RSVP BCI Framework

- 1) Experiment and Data Preparation: RSVP is an event-related highly efficient BCI technique for examining visual perception and is helpful in detecting target and nontarget stimulus events. The RSVP experiment was designed to detect the target object in a multitarget scenario proposed by Ko et al. [2]. The experiment is recorded at a 500-Hz sampling rate using a 32-channel Neuroscan system, which consists of seven sessions with each session containing a 1-min rest state followed by 32 trials. Each trial is composed of fixation, searching, and stimulus stages. The experimental design randomly highlights four icons in a grid of size 8×8 during each trial, in which one of them is a target event icon. The icons were flickered at randomly allocated preallocated frequencies of 4, 5, 6, and 7 Hz, and the subjects are intended to focus on the target event icon and detect all the match-three possible events in each trial. The experiment was designed such that the target object appears only three times during the stimulus phase. Fourteen subjects participated in the study in accordance with the recommendations from the NYCU-REC committee, Hsinchu, Taiwan, under the protocol code NCTU-REC-104-033. All the recorded trials across sessions were BPF filtered between 1 and 50 Hz, and concatenated subjectwise for ASR processing.
- 2) Feature Extraction and Classification: Event-related potentials (ERPs) were extracted for the target and nontarget events from the ASR processed EEG trials in line with the previous study [2]. Target event ERP of 1 s is extracted by selecting -200- to 800-ms duration with respect to the target event onset, while nontarget event ERP picks 0 to 1000 ms without overlapping the target event onset. The subjectwise target and nontarget ERPs were labeled accordingly for classification analysis. Furthermore, the discrimination performance between target and nontarget events was analyzed using the bootstrap aggregating (Bagging) tree algorithm, which is a supervised ensemble learning method based on the decision tree mechanism. The leave-one-subject-out cross-validation

(LOSOCV) approach is applied to evaluate the classification performance.

D. MI BCI Framework

- 1) Experiment and Data Preparation: The MI dataset evaluated in this study was published by Kaya et al. [46]. EEG signals were recorded using EEG-1200 JE-921A EEG system (Nihon Kohden, Japan) based on standard 10/20 international configuration using 19 channels (Fp1, F3, F7, C3, P3, T3, T5, Fz, Cz, Pz, Fp2, F4, F8, C4, P4, T4, T6, O1, and O2). The sampling frequency was 200 Hz, and the impedance was maintained below 10 k Ω . The dataset consists of hand, foot, and tongue MI activities, in which hand MI is considered for this study. Thirteen healthy subjects participated in the study. During the experiment, subjects were instructed to focus toward the fixation point placed at the center of the screen where a stimulation signal indicating left hand or right hand or circle of 1 s was presented. The subjects perform the MI task by imagining the closing and opening of the fist according to the direction of the stimulus within that period or remain passive when the circle is stimulated. A total of 9224 MI trials were recorded across all the subjects, and an 8–50-Hz BPF filter is applied. All the recorded trials were concatenated subjectwise and performed ASR processing to remove the artifact components.
- 2) Feature Extraction and Classification: Functional connectivity features were shown to enable the classification of upper and lower limb MI [47], [48]. Pearson's correlation (13) was used to measure the pairwise correlation of EEG signals between pairs of electrodes. Therefore, the reconstructed MI EEG dataset was feature extracted using the Pearson correlation to analyze the functional connectivity between the electrode pairs. The number of extracted features obtained was $C \times C$, where C is the number of recording electrodes. The linear support vector machine (SVM) was used to classify the connectivity features extracted from left and right hand MIs. The SVM was trained with ten-fold cross-validation to evaluate the classification performance. The random guessing threshold for two-class classification was maintained to be 50%.

IV. RESULTS

A. Benchmark Dataset

1) Average Eye and Muscle Activity: The average proportions of EOG and EMG components in the clean and contaminated EEG signals are observed by applying a powerful tool, ICLabel [49]. ICLabel is an automatic independent component (IC) classifier that applies efficient neural network models that are rigorously trained on a wide variety of ICs extracted from millions of EEG datasets that are carefully labeled by EEG experts. This trained model classifies the IC classes across seven labels (brain, muscle, eye, heart, line noise, channel noise, and others). In this study, we analyzed the ICs from the clean, EOG, and EMG contaminated EEG signals and applied ICLabel to classify the projections of each component across the subjects. Fig. 4 shows the projections of the brain, eye, and muscle components from the three datasets.

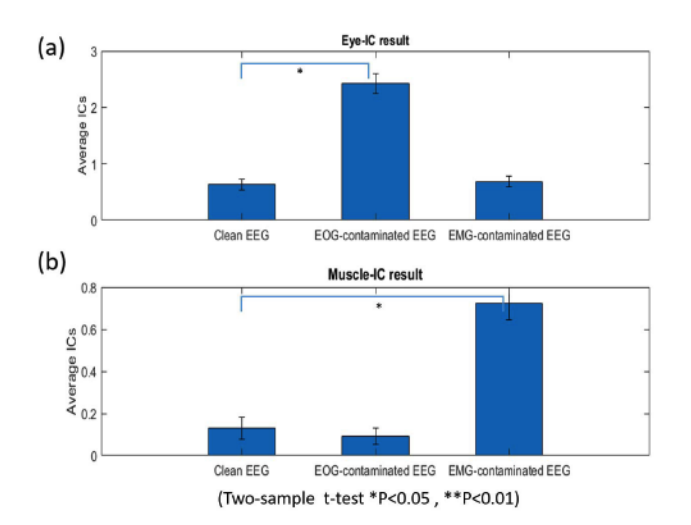


Fig. 4. Classification result using ICLabel across subjects. (a) Average number of eye-components in EEG/EOG signal. (b) Average number of muscle-components in EEG/EMG signal.

The average number of eye-activity-related components was 2.5 in the EOG-contaminated dataset (p < 0.05), which is greater than the clean EEG and EEG/EMG datasets (0.58 and 0.62), as shown in Fig. 4(a). Fig. 4(b) shows the average muscle-activity components of 0.77 in the EMG-contaminated EEG dataset (p < 0.05), which is significantly greater than clean EEG and EEG/EOG datasets (0.19 and 0.16). The results across all the subjects show that eye and muscle-activity components in the EEG/EOG and EEG/EMG datasets are significantly dominant.

2) Root-Mean-Square Error (RMSE): RMSE is calculated between the clean and processed EEG data to evaluate the efficacy of the artifact removal mechanism between different ASR methods. Fig. 5 shows the box plot representation of EOG and EMG artifacts projected onto the clean EEG signals. Since the projection matrix is superimposed on the frontal region for EOG and on either side of the temporal region for EMG contamination, their strengths are localized to those regions only. Therefore, the RMSE and SNR evaluations are performed for the electrode combinations that are localized in the frontal and temporal regions. The electrode channels considered for EOG analysis are Fp1, Fp2, F3, and F4 and, for EMG analysis, are T3, T4, T5, and T6. The first column in Fig. 5 represents the calculated average RMSE between the clean and processed EEG signals using Init-ASR, MW-ASR, PSP-ASR, and PSW-ASR algorithms for both EOG and EMG contaminations when c = 20. These box plots show that PSP-ASR and PSW-ASR algorithms attained lower average RMSE values of 6.66 (± 3.75) and 4.52 (± 3.03) for EEG/EOG, and 1.08 (± 0.5) and 0.94 (± 0.47) for EEG/EMG signals compared to Init-ASR and MW-ASR methods, 7.15 (± 4.13) and 7.98 (± 4.85) for EEG/EOG, and 1.18 (± 0.56) and 1.29 (± 0.59) for EEG/EMG signal across the subjects. Furthermore, PSW-ASR showed improved performance by maintaining minimum variance between the subjects and significantly lower RMSE values compared to other algorithms.

3) Signal-to-Noise Ratio (SNR): The projection of the desired clean EEG signal onto the artifact components was examined by calculating the channelwise SNR across the

subjects. The second column in Fig. 5 shows the box representation of averaged SNR power processed by the Init-ASR, MW-ASR, PSP-ASR, and PSW-ASR algorithms for EOG and EMG-contaminations when c=20. Higher SNR powers of 5.74 (± 3.93) and 8.63 (± 2.88) for EEG/EOG, and 16.61 (± 3.29) and 17.9 (± 2.92) for EEG/EMG signals were observed using PSP-ASR and PSW-ASR compared to Init-ASR and MW-ASR algorithms with 5.13 (± 4.24) and 4.43 (± 4.63) for EEG/EOG, and 15.89 (± 3.84) and 15.07 (± 3.7) for EEG/EMG signals. Similar to RMSE results, PSW-ASR reported significantly improved SNR power between subjects for both EEG/EOG and EEG/EMG signals confirming reduced noise power, which resembles that PSW-ASR is more consistent in removing artifacts across the subjects than PSP-ASR.

Through visual inspection, we still observe eye and muscle activity components in the EEG signal even after PSP-ASR and PSW-ASR processing. However, the percentage of eye and muscle activity powers was significantly reduced compared to Init-ASR and MW-ASR. This shows that the adaptive learning mechanism improved the quality of signal reconstruction and, therefore, can be treated as a better choice to employ as an artifact removal technique, especially in activity-specific EEG experimental designs, which might further help in improving the BCI performance. Furthermore, the presence of artifacts might also be due to the choice of the c value that determines the quality of the artifact removal. Fig. 5 is evaluated for c=20 and a statistical significance of p<0.05 using the Wilcoxon signed-rank test.

B. SSVEP BCI Framework

1) Pearson Correlation: To evaluate the similarity between data processed by online ASR and the ground-truth data obtained from off-line ASR, their correlations were analyzed across the subjects. Fig. 6 shows the channelwise average Pearson correlation similarity between the processed data obtained from the Init-ASR, MW-ASR, PSP-ASR, and PSW-ASR and the ground-truth data. The channelwise results show that PSP-ASR and PSW-ASR algorithms obtained maximum correlation values compared to the Init-ASR and MW-ASR algorithms (p < 0.05). Furthermore, notable differences in the correlation value between methods are observed for the channels that are mounted in the frontal region. Fig. 7(a)–(d) shows the channelwise correlation performance across the subjects, which infers that the frontal regions, especially Fp1 and Fp2 electrodes, might be contaminated by the eye activity components. The correlation matrix also shows that adaptive learning algorithms, such as PSP-ASR and PSW-ASR, outperformed in the frontal regions compared to Init-ASR and MW-ASR confirming their efficient artifact removal ability. The average Pearson correlation values at the Fp1 electrode are 0.81 (± 0.2) , 0.82 (± 0.2) , 0.88 (± 0.1) , and 0.89 (± 0.1) , and those of Fp2 electrode are 0.80 (\pm 0.2), 0.82 (\pm 0.19), 0.89 (\pm 0.086), and 0.89 (± 0.096) when evaluated between ground-truth data and Init-ASR, MW-ASR, PSP-ASR, and PSW-ASR processed data, respectively. In addition, Fig. 7(e) and (f) demonstrates the topological representation of calculated correlation coefficients for the best and worst case scenarios, and Fig. 7(g)

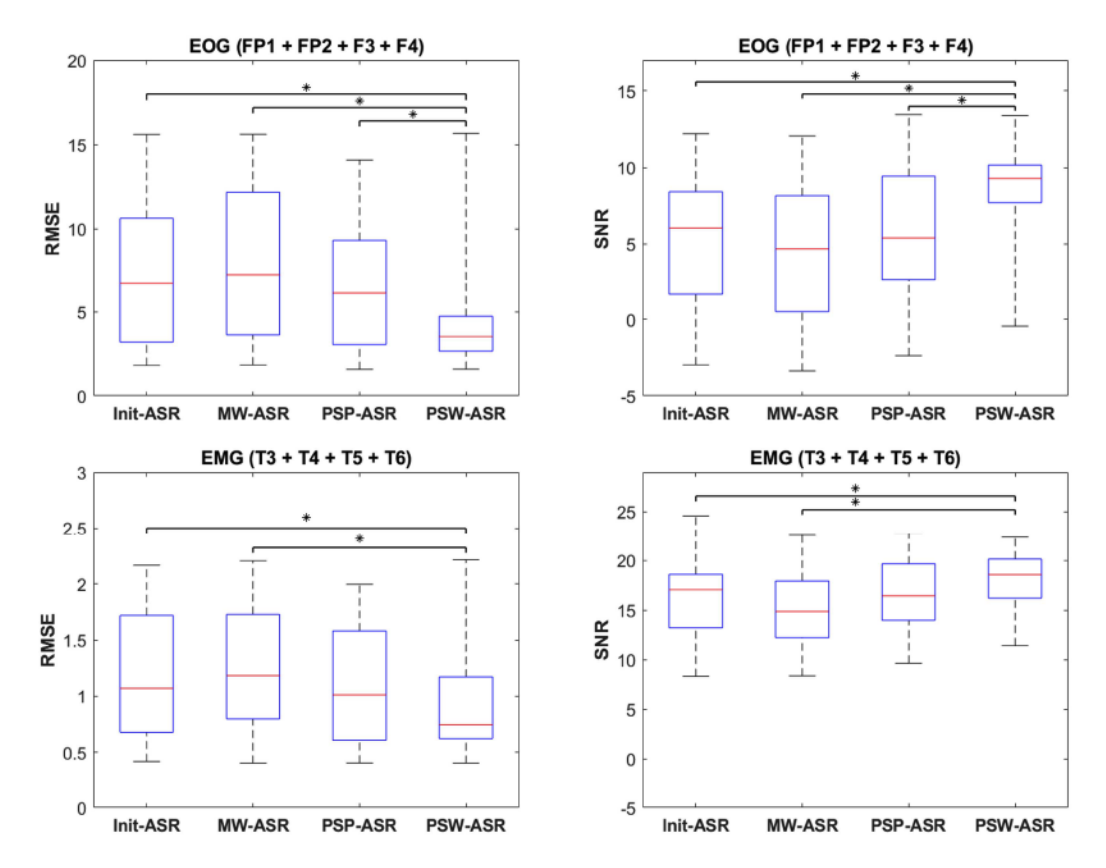


Fig. 5. Box plot representation of the average RMSE and SNR for EEG/EOG signal with eye activity artifacts projected onto the scalp frontal region electrodes (top row) and EEG/EMG signal with muscle activity artifacts projected onto either side of the scalp temporal region electrodes (bottom row). All the algorithms were processed for c = 20. SNR is evaluated in decibels (dB). The red line in the interquartile range (box) indicates the median value, and the whisker in dotted lines represents the range between min(.) and max(.) values. * indicates p < 0.05.

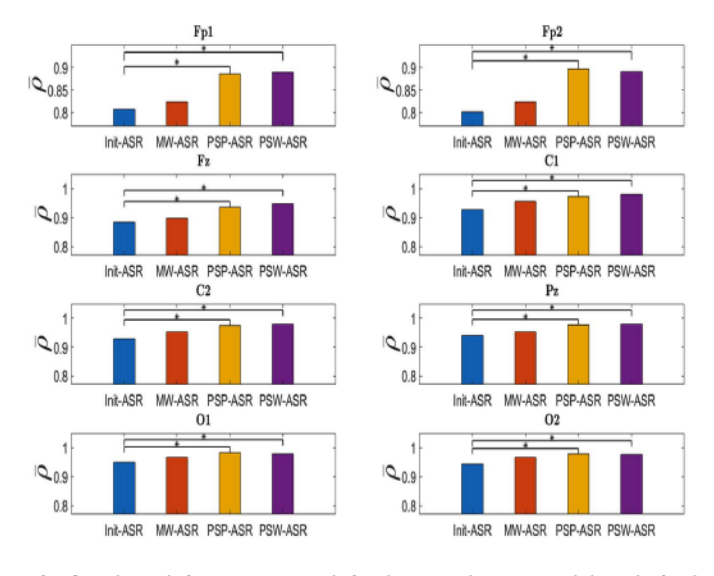


Fig. 6. Channelwise average correlation between the processed data obtained from Init-ASR, MW-ASR, PSP-ASR, PSW-ASR, and ground truth obtained from off-line ASR. * indicates p < 0.05.

shows the average correlation across all the subjects. The best case is obtained for subject 2 and the worst case for subject 13. Although the correlation difference between ASR methods is not quite different in the central, parietal, and occipital regions, PSP-ASR and PSW-ASR showed better performance compared to init-ASR and MW-ASR, as shown in Fig. 6.

2) Accuracy: Accuracy is another indicator of evaluating the SSVEP performance at each stimulus frequency. The performance is analyzed for a range of c values to estimate the efficacy of the proposed models. Fig. 8 shows the average classification accuracy of the target frequency obtained by evaluating the DP to the reconstructed artifact subspace using off-line ASR, Init-ASR, MW-ASR, PSP-ASR, and PSW-ASR algorithms. Furthermore, average DP accuracy is also calculated for the raw EEG signal as a reference, which is highlighted using a red horizontal line. The results implicate higher PSW-ASR performance for the aggressive choice of c = 1 to 3 values with a maximum accuracy of 89.56% when c = 1. PSP-ASR and MW-ASR achieved maximum accuracy of 88.67% and 87.56 when c = 1, and Init-ASR performed well for the range of c = 4 to 12 with a maximum accuracy of 88% when c = 4. The standard off-line ASR performed consistently across c values with a maximum accuracy of 86.44% when c=6. In addition, there are no significant performance differences between the ASR methods for c > 13. On the contrary, an increasing pattern in performance is observed for Init-ASR and PSW-ASR algorithms when c < 13 confirming that a proper choice of c value is extremely crucial for determining the efficacy of the proposed algorithm in signal reconstruction. Overall, the results showed an improved BCI performance for the aggressive choice of c values (c = 1 to 3) when PSW-ASR is applied, which demonstrated the ability of Hebbian/anti-Hebbian networks in tracking the EEG dynamics effectively.

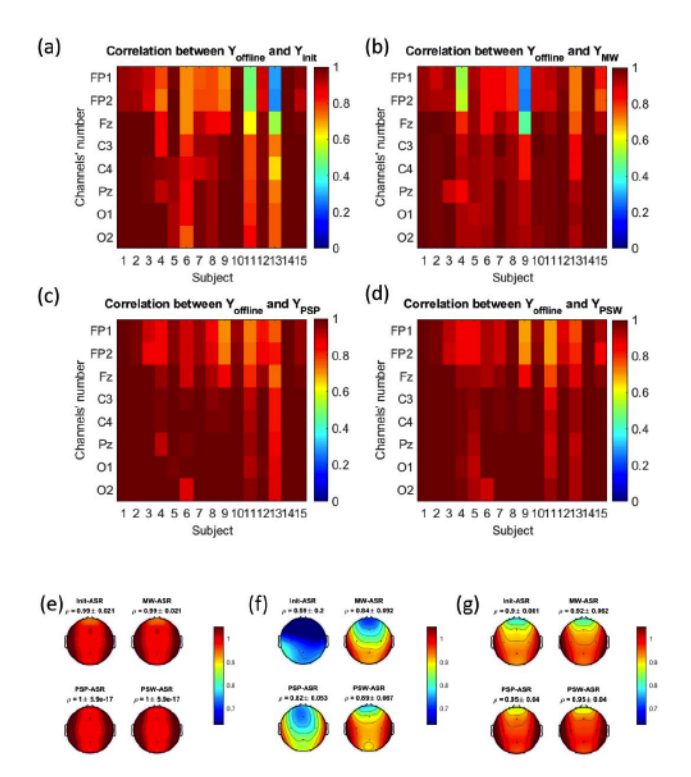


Fig. 7. 8×15 Correlation matrix to visualize the subjectwise Pearson correlation between off-line ASR and (a) Init-ASR, (b) MW-ASR, (c) PSP-ASR, and (d) PSW-ASR across all the channels. The topological representation of correlation for subjects' with (e) best case (#2), (f) worst case (#13) and (g) average case scenario. # indicates the experimental subject.

Although the classification accuracy of PSW-ASR is not dominant across the range of c values (c > 3), it produced consistent accuracy levels that are always greater than the reference DP classification accuracy.

C. RSVP BCI Framework

During RSVP, the functional differences in the brain are significantly observed between the target and nontarget stimulations through the propagation of p300 activations approximately at 300 ms after the target event onset, which is the largest positive peak of the ERP waveform. The target and nontarget ERP features obtained from the reconstructed EEG signals using Init-ASR and PSW-ASR are applied to the Bagging tree binary classifier to evaluate the classification performance by distinguishing the target and nontarget events through the LOSOCV cross-validation mechanism. The classification results demonstrated higher PSW-ASR performance than Init-ASR across the range of c = 1 to 20 values. Further observations showed that PSW-ASR exhibited maximum accuracy of 80.82% when c = 5, which is significantly (p < 0.01) higher than 72.64% observed using Init-ASR, when c = 5, which is shown in Table I. Alternatively, Init-ASR exhibited maximum accuracy of 78.56% when c = 20, which is lower than 80.06% using the PSW-ASR algorithm. Finally, the overall empirical results showed that the aggressive choice of c values (c < 8) in PSW-ASR significantly (p < 0.01) discriminated the target and nontarget events compared to Init-ASR and illustrates that the adaptive ASR mechanism efficiently tracks the dynamics of the EEG signals.

D. MI BCI Framework

The ASR reconstructed left and right hand MI trials were featured extracted by evaluating the pairwise Pearson correlation across the channels. Furthermore, the extracted features were fed into the SVM binary classifier to distinguish the MI activity. The results from Table I showed that the PSW-ASR algorithm improved the BCI performance in discriminating the left and right hand activities compared to Init-ASR. In particular, PSW-ASR exhibited significantly (p < 0.05) higher accuracy of 71.05% compared to 67.73% using Init-ASR when c = 10. Although PSW-ASR dominated the Init-ASR algorithm across the range of c values (c = 1 to 20), the aggressive choice of c < 10 produced significant (p < 0.05) improvement in PSW-ASR. Interestingly, Init-ASR observed comparable performance with PSW-ASR for higher c values (c > 15), where the artifact removal is not strict enough. These findings implicate that the aggressive choice of c < 10 range in PSW-ASR retained the activity-specific brain signals while removing the artifact components resembling that the adaptive mechanism introduced using Hebbian/anti-Hebbian learning networks is quite useful in understanding the dynamic patterns of activity-specific brain signals.

V. DISCUSSION

BCI technology often suffers from performance degradation caused by physiological and nonphysiological artifacts during the EEG acquisition process, which needs to be addressed with utmost care. However, assessing a clean artifact subspace from the entire EEG dataset is impractical in online BCI applications. On the other hand, using a fixed artifact subspace from the initial segment of the EEG data may hinder the performance of artifact removal. Although conventional movingwindow-based techniques (MW-ASR) provide comparatively better results by independently updating the segmentwise artifact subspace, the method lacks in its ability to optimize efficiently by tracking the subspace and update adaptively. Thus, a technique that can adaptively learn and optimize the artifact subspace by effectively reducing the dimensionality of the streaming data is required. As the dimensionality of the streaming input typically reduces during the early sensory processing of the neural network models by learning the principal subspace in accordance with the activity-dependent learning rules, the PSP and PSW algorithms derived from Hebbian/anti-Hebbian neural networks are quite useful [30], [32]. This study proposes an adaptive subspace tracking mechanism that updates the learning parameters segment-bysegment based on the dynamics of the EEG signals. The results showed that the PSW-ASR algorithm performed well for the Benchmark dataset, and SSVEP, RSVP, and MI BCI frameworks, which could be a potential choice of artifact-removal mechanism that might further improve the performance in BCI applications.

A. Adaptive Mechanism of Artifact Subspace

The standard ASR and Riemannian ASR (rASR) algorithms require calibration data under a resting condition recorded separately at the beginning of the session [24], [26]. Hence,

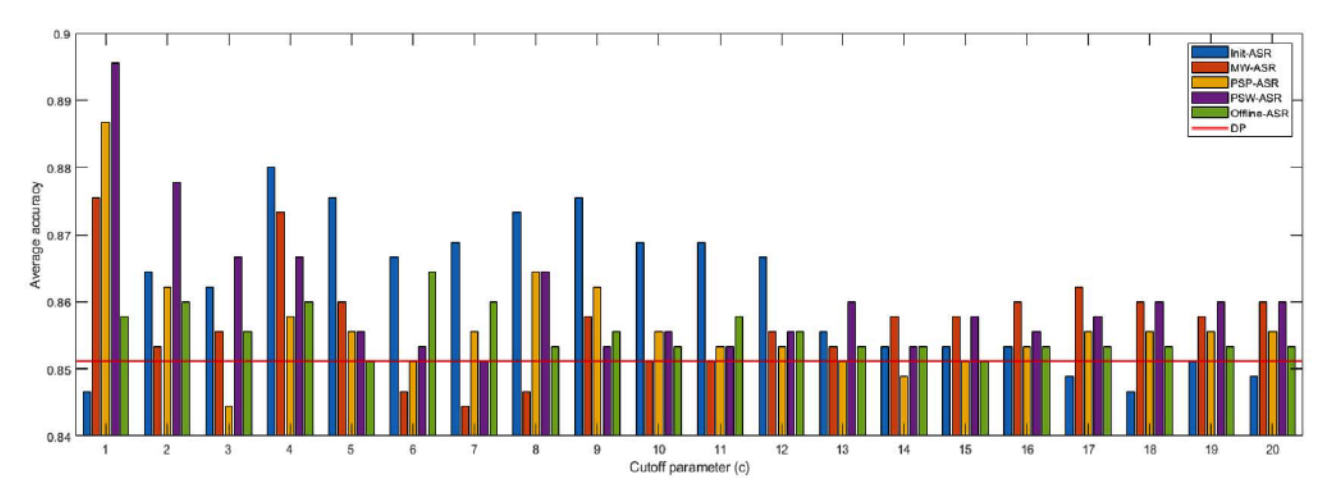


Fig. 8. Performance enhancement of SSVEP BCI system processed using off-line ASR, Init-ASR, MW-ASR, PSP-ASR, and PSW-ASR algorithms for different c values. The red horizontal bar represents the classification performance of EEG signal evaluated using DP without any ASR cleaning process.

TABLE I PERFORMANCE SUMMARY OF INIT-ASR AND PSW-ASR ON SSVEP, RSVP, AND MI BCI FRAMEWORKS. # INDICATES THE NUMBER, $c_{\rm OPTIMAL}$ INDICATES THE OPTIMAL c Value, * Indicates p < 0.05, and ** Indicates p < 0.01

	$SSVEP_{[44]}$	$RSVP_{[2]}$	$MI_{[46]}$
BCI Type	Visual stimulus	P300	Left/right hand motor imagery
# of subjects	15	14	13
# of trials	450	18816	9224
# of channels	8	9	19
Features	SSVEP	ERP	Pearson Correlation
Classification method	Differentiable power	Bagging Tree	Support vector machine (SVM)
$c_{optimal}$	1	5	10
Init-ASR (%)	84.6 ± 9	72.64 ± 13.58	67.63 ± 3.18
PSW-ASR (%)	89.6 ± 7.7*	80.82 ± 5.39**	71.05 ± 2.35*
Performance improvement (%)	4.69 ± 8.82	8.58 ± 14.9	1.73 ± 2.17
Significance (p)	Paired t-sest	Paired t-test	Paired t-test

the quality of the artifact removal depends on the quality of the calibration data and the type of artifacts in the EEG signal. However, in real-time BCI applications, these initial settings for calibration are not feasible, and the methods that can automatically extract reference subspace are needed. Considering the limitations of fixed artifact subspace, Hebbian/anti-Hebbian neural networks continuously update the artifact subspace by learning and adjusting the synaptic weights based on the feedforward and lateral synaptic weight matrices. The network tracks the principal subspace of the segmentwise nonstationary EEG data and adapts to the varying distributions thereby updating the W and Msynaptic weight matrices that are further projected onto the ASR algorithm to update M_r and T_i values. This adaptive learning mechanism using Hebbian/anti-Hebbian networks on the ASR algorithm leads to PSP-ASR, and adding a constraint that normalizes the principal subspace in the objective function gives PSW-ASR. The superiority of these adaptive algorithms can be observed in Fig. 5 for the benchmark dataset and in Table I for SSVEP, RSVP, and MI BCI frameworks. The average RMSE and SNR of the eye-blink and muscle activities projected onto the brain-specific region for the benchmark

dataset showed the advantage of using Hebbian/anti-Hebbian learning networks. Similarly, our proposed adaptive learning mechanism improved the classification performance across the three BCI frameworks compared to the conventional Init-ASR method. This showed that the adaptive subspace tracking mechanism using Hebbian/anti-Hebbian neural networks learns the dynamics of the signal efficiently, thereby increasing the reliability of the ASR algorithm.

B. Constrained Learning With Hebbian/Anti-Hebbian Neural Network

Equalization or whitening is essential to suppress the spatiotemporal correlation in the signals that are contaminated by various sources, which are actively observed in multichannel EEG analysis [50], [51]. Thus, the objective function of the PSP algorithm derived from the Hebbian/anti-Hebbian learning network is equalized by optimally projecting the streaming data onto its principal subspace by enforcing feedforward and lateral learning rules, resulting in a constraint on the PSP algorithm, namely, PSW. This derived whitening constraint normalizes the output variance in all directions, thereby regularizing the principal subspace. [30], and established clear

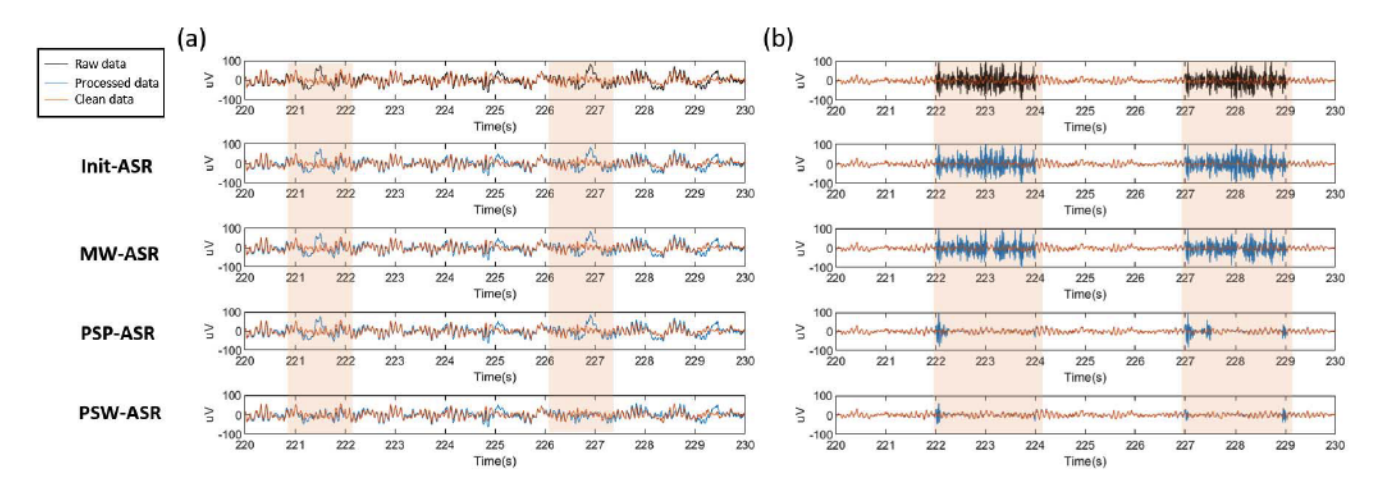


Fig. 9. Comparison of subspace tracking mechanism under (a) EOG contamination at Fp1 channel and (b) EMG contamination at T3 channel for subject-16. The top row shows the clean (orange) and contaminated raw (black) EEG signal before processing. The resultant EEG signals processed by Init-ASR, MW-ASR, PSP-ASR, and PSW-ASR are shown in blue.

boundary conditions for the choice of learning rates r_W , r_M , r_W' , and r_M' to maintain the stability and convergence of the PSP and PSW algorithms. In this study, the learning parameters are chosen based on the recommendations from [30], thereby ensuring the convergence of PSP and PSW algorithms. The whitening mechanism in PSW-ASR provided superior performance for all the experimental scenarios by robustly influencing the W and M synaptic weights onto the M_r and T_i parameters of the ASR algorithm.

Fig. 9 shows the projection of the subspace tracking mechanism obtained from different online ASR methods onto clean EEG data for the benchmark dataset contaminated by EOG and EMG artifacts for c=20. The results demonstrate that our proposed Hebbian/anti-Hebbian learning mechanism removed the artifact components efficiently without corrupting the EEG signal compared to the conventional ASR methods. Further observations showed that the PSW-ASR algorithm outperformed the other three methods by robustly removing eye and muscle artifact components.

C. Cutoff Parameter Adjustment in SSVEP BCI Application

The standard ASR algorithm proposed by [24] validates the significance of cutoff parameter c and suggested their optimal choice (c_{optimal}) between 20 and 30 for general BCI applications. In addition, the authors also analyzed the percentage reduction power of artifacts and brain components after ASR cleaning for different ranges of c values and deduced that, when c < 20, more brain components were affected, and the ratio of removing artifact components to the brain components deteriorated. However, [52], [53] demonstrated the possibility of choosing aggressive cutoff parameters to remove artifacts, especially for improving BCI performance in activity-specific BCI applications. Fig. 8 and Table I showed the detection accuracy of the SSVEP, RSVP, and MI BCI frameworks across different cutoff parameters. The results showed the effectiveness of the PSW-ASR algorithm for the choice of aggressive c value range (c = 1 to 10). Although aggressive cutoff might lead to decreased power of brain signals after reconstruction [24], the enhanced BCI performance of the PSW-ASR algorithm for aggressive c values showed that the

activity-specific brain signals were retained efficiently after the artifact removal, which enables the potential of adaptive learning mechanism through Hebbian/anti-Hebbian neural networks.

VI. CONCLUSION

This study proposed an online capable adaptive artifact subspace mechanism by integrating Hebbian/anti-Hebbian neural networks into the ASR algorithm resulting in PSP-ASR and PSW-ASR. Our adaptive ASR algorithm eliminates the problem of fixed reference data for calibration [24], [26] by continuously updating the artifact subspace segmentwise and automatically adjusting the synaptic weights of the network through an adaptive learning mechanism. Our results from the benchmark dataset, and SSVEP, RSVP, and MI BCI frameworks confirmed that the adaptive ASR algorithm displayed significant performance improvements in removing the artifact components and retaining the brain activities efficiently by modifying the standard choices in the ASR algorithm. Constraining the principal subspace by whitening (PSW) decorrelates the feedforward and lateral synaptic weights, and regularizes the principal subspace, which robustly improves the artifact subspace tracking. Our empirical results suggested that the choice of the cutoff parameter plays an important role in determining the quality of the artifact reduction and signal reconstruction. Furthermore, our algorithm showed that the activity-specific BCI experiments exhibited significant performance improvements during aggressive threshold conditions in the range c = 1 to 10, which confirmed the ability of PSW-ASR in preserving the task-specific brain activity components compared to Init-ASR. The study also showed that PSW-ASR produced comparable results for a moderate range of c values, deducing its reliability in general BCI applications.

Future work will be focused on analyzing the BCI performance by applying the proposed adaptive learning mechanism to other biologically plausible artifacts and further validating its agility in clinical applications.

ACKNOWLEDGMENT

The authors would like to thank C.-R. Phang, Y. Chang, and C.-H. Su, Ph.D. students at National Yang Ming Chiao Tung

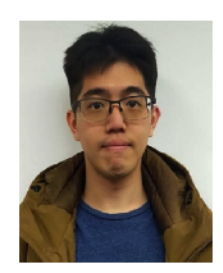
University, for helping to evaluate our proposed algorithm across different BCI frameworks.

REFERENCES

- Y. Zhang et al., "Improving EEG decoding via clustering-based multitask feature learning," IEEE Trans. Neural Netw. Learn. Syst., early access, Feb. 8, 2021, doi: 10.1109/TNNLS.2021.3053576.
- [2] L.-W. Ko et al., "SSVEP-assisted RSVP brain-computer interface paradigm for multi-target classification," J. Neural Eng., vol. 18, no. 1, 2020, Art. no. 016021.
- [3] U. Chaudhary, N. Birbaumer, and A. Ramos-Murguialday, "Brain-computer interfaces for communication and rehabilitation," *Nature Rev. Neurol.*, vol. 12, no. 9, pp. 513–525, 2016.
- [4] J. C. Henry, "Electroencephalography: Basic principles, clinical applications, and related fields," *Neurology*, vol. 67, no. 11, p. 2092, 2006.
 [5] M. Sazgar and M. G. Young, "Seizures and epilepsy," in *Absolute*
- [5] M. Sazgar and M. G. Young, "Seizures and epilepsy," in Absolute Epilepsy and EEG Rotation Review. Cham, Switzerland: Springer, 2019, pp. 9–46.
 [6] X. Jiang, G.-B. Bian, and Z. Tian, "Removal of artifacts from EEG
- [6] X. Jiang, G.-B. Bian, and Z. Tian, "Removal of artifacts from EEG signals: A review," *Sensors*, vol. 19, no. 5, p. 987, 2019.
 [7] J. Urigüen and B. Garcia-Zapirain, "EEG artifact removal-state-of-the-
- [7] J. Urigüen and B. Garcia-Zapirain, "EEG artifact removal-state-of-theart and guidelines," J. Neural Eng., vol. 12, no. 3, 2015, Art. no. 031001.
- [8] T. J. Huppert, S. G. Diamond, M. A. Franceschini, and D. A. Boas, "HomER: A review of time-series analysis methods for near-infrared spectroscopy of the brain," *Appl. Opt.*, vol. 48, no. 10, p. D280, 2009.
- [9] M. K. Islam, A. Rastegarnia, and Z. Yang, "Methods for artifact detection and removal from scalp EEG: A review," *Clin. Neurophysiol.*, vol. 46, nos. 4–5, pp. 287–305, 2016.
- [10] C.-T. Lin et al., "Review of wireless and wearable electroencephalogram systems and brain-computer interfaces—A mini-review," Gerontology, vol. 56, no. 1, pp. 112–119, 2010.
- vol. 56, no. 1, pp. 112–119, 2010.
 [11] C.-T. Lin et al., "Wearable and wireless brain-computer interface and its applications," in *Proc. Int. Conf. Found. Augmented Cognition*, Jul. 2009, pp. 741–748.
- pp. 741–748.
 [12] S. P. Fitzgibbon, D. M. W. Powers, K. J. Pope, and C. R. Clark, "Removal of EEG noise and artifact using blind source separation," *J. Clin. Neurophysiol.*, vol. 24, no. 3, pp. 232–243, 2007.
- [13] T. P. Jung et al., "Removing electroencephalographic artifacts by blind source separation," Psychophysiology, vol. 37, no. 2, pp. 163–178, Mar 2000
- [14] M. T. Akhtar, W. Mitsuhashi, and C. J. James, "Employing spatially constrained ICA and wavelet denoising, for automatic removal of artifacts from multichannel EEG data," *Signal Process.*, vol. 92, no. 2, pp. 401–416, 2012.
- pp. 401–416, 2012.
 [15] I. Winkler, S. Haufe, and M. Tangermann, "Automatic classification of artifactual ICA-components for artifact removal in EEG signals," *Behav. Brain Funct.*, vol. 7, no. 1, p. 30, Aug. 2011.
- [16] S. Casarotto, A. M. Bianchi, S. Cerutti, and G. A. Chiarenza, "Principal component analysis for reduction of ocular artefacts in event-related potentials of normal and dyslexic children," *Clin. Neurophysiol.*, vol. 115, no. 3, pp. 609–619, Mar. 2004.
- [17] G. L. Wallstrom et al., "Correction of ocular artifacts in the EEG using Bayesian adaptive regression splines," in Case Studies in Bayesian Statistics, New York, NY, USA: Springer, 2002, pp. 351-365.
- Statistics. New York, NY, USA: Springer, 2002, pp. 351–365.
 [18] B. Noureddin, P. D. Lawrence, and G. E. Birch, "Online removal of eye movement and blink EEG artifacts using a high-speed eye tracker," *IEEE Trans. Biomed. Eng.*, vol. 59, no. 8, pp. 2103–2110, Aug. 2012.
- [19] T. T. H. Pham, R. J. Croft, P. J. Cadusch, and R. J. Barry, "A test of four EOG correction methods using an improved validation technique," *Int. J. Psychophysiol.*, vol. 79, no. 2, pp. 203–210, Feb. 2011.
- [20] Z. Wu and N. E. Huang, "Ensemble empirical mode decomposition: A noise-assisted data analysis method," Adv. Adapt. Data Anal., vol. 1, no. 1, pp. 1–41, Jan. 2009.
- [21] X. Xu, X. Chen, and Y. Zhang, "Removal of muscle artefacts from few-channel EEG recordings based on multivariate empirical mode decomposition and independent vector analysis," *Electron. Lett.*, vol. 54, no. 14, pp. 866–868, 2018.
- [22] C. A. E. Kothe and T.-P. Jung, "Artifact removal techniques with signal reconstruction," U.S. Patent App. 14895440, Apr. 28, 2016.
 [23] A. Delorme and S. Makeig, "EEGLAB: An open source toolbox for
- [23] A. Delorme and S. Makeig, "EEGLAB: An open source toolbox for analysis of single-trial EEG dynamics including independent component analysis," *J. Neurosci. Methods*, vol. 134, no. 1, pp. 9–21, Mar. 2004.
- [24] C.-Y. Chang, S.-H. Hsu, L. Pion-Tonachini, and T.-P. Jung, "Evaluation of artifact subspace reconstruction for automatic artifact components removal in multi-channel EEG recordings," *IEEE Trans. Biomed. Eng.*, vol. 67, no. 4, pp. 1114–1121, Apr. 2020.

- [25] P. Anders et al., "The influence of motor tasks and cut-off parameter selection on artifact subspace reconstruction in EEG recordings," Med. Biol. Eng. Comput., vol. 58, pp. 2673–2683, Aug. 2020.
- [26] S. Blum, N. S. J. Jacobsen, M. G. Bleichner, and S. Debener, "A Riemannian modification of artifact subspace reconstruction for EEG artifact handling," *Frontiers Hum. Neurosci.*, vol. 13, p. 141, Apr. 2019.
- [27] B. Yang, "Projection approximation subspace tracking," *IEEE Trans. Signal Process.*, vol. 43, no. 1, pp. 95–107, Jan. 1995.
- [28] K. I. Diamantaras and S. Y. Kung, Principal Component Neural Networks: Theory and Applications. Hoboken, NJ, USA: Wiley, 1996.
- [29] R. Arora, A. Cotter, K. Livescu, and N. Srebro, "Stochastic optimization for PCA and PLS," in *Proc. 50th Annu. Allerton Conf. Commun.*, Control, Comput. (Allerton), Oct. 2012, pp. 861–868.
- [30] C. Pehlevan, A. M. Sengupta, and D. B. Chklovskii, "Why do similarity matching objectives lead to Hebbian/anti-Hebbian networks?" *Neural Comput.*, vol. 30, no. 1, pp. 84–124, Jan. 2018.
- [31] N. Kermiche, "Contrastive Hebbian feedforward learning for neural networks," *IEEE Trans. Neural Netw. Learn. Syst.*, vol. 31, no. 6, pp. 2118–2128, Jun. 2020.
- [32] C. Pehlevan, T. Hu, and D. B. Chklovskii, "A Hebbian/anti-Hebbian neural network for linear subspace learning: A derivation from multidimensional scaling of streaming data," *Neural Comput.*, vol. 27, no. 7, pp. 1461–1495, 2015.
- [33] T. Hu et al., "A Hebbian/anti-Hebbian network for online sparse dictionary learning derived from symmetric matrix factorization," in Proc. 48th Asilomar Conf. Signals, Syst. Comput., Nov. 2014, pp. 613–619.
- [34] A. Giovannucci, V. Minden, C. Pehlevan, and D. B. Chklovskii, "Efficient principal subspace projection of streaming data through fast similarity matching," in *Proc. IEEE Int. Conf. Big Data (Big Data)*, Dec. 2018, pp. 1015–1022.
- [35] E. Oja, "Neural networks, principal components, and subspaces," Int. J. Neural Syst., vol. 1, no. 1, pp. 61–68, 1989.
- [36] T. D. Sanger, "Optimal unsupervised learning in a single-layer linear feedforward neural network," *Neural Netw.*, vol. 2, no. 6, pp. 459–473, 1989.
- [37] C.-Y. Chang, S.-H. Hsu, L. Pion-Tonachini, and T.-P. Jung, "Evaluation of artifact subspace reconstruction for automatic EEG artifact removal," in *Proc. 40th Annu. Int. Conf. IEEE Eng. Med. Biol. Soc. (EMBC)*, Jul. 2018, pp. 1242–1245.
- [38] L. Pion-Tonachini, S.-H. Hsu, C.-Y. Chang, T.-P. Jung, and S. Makeig, "Online automatic artifact rejection using the real-time EEG source-mapping toolbox (REST)," in *Proc. 40th Annu. Int. Conf. IEEE Eng. Med. Biol. Soc. (EMBC)*, Jul. 2018, pp. 106–109.
- [39] M. A. Klados and P. D. Bamidis, "A semi-simulated EEG/EOG dataset for the comparison of EOG artifact rejection techniques," *Data Brief*, vol. 8, pp. 1004–1006, Sep. 2016.
- [40] A. Hamilton-Wright and D. W. Stashuk, "Physiologically based simulation of clinical EMG signals," *IEEE Trans. Biomed. Eng.*, vol. 52, no. 2, pp. 171–183, Feb. 2005.
- [41] S. D. Muthukumaraswamy, "High-frequency brain activity and muscle artifacts in MEG/EEG: A review and recommendations," Frontiers Hum. Neurosci., vol. 7, p. 138, Apr. 2013.
- [42] I. I. Goncharova, D. J. McFarland, T. M. Vaughan, and J. R. Wolpaw, "EMG contamination of EEG: Spectral and topographical characteristics," *Clin. Neurophysiol.*, vol. 114, no. 9, pp. 1580–1593, Sep. 2003.
- [43] D. Sandeep Vara Sankar and L.-W. Ko, "Evaluation of fatigue and attention levels in multi-target scenario using CNN," in *Proc. Int. Comput. Symp. (ICS)*, Dec. 2020, pp. 247–251.
- [44] L.-W. Ko et al., "Development of a smart helmet for strategical BCI applications," Sensors, vol. 19, no. 8, p. 1867, Apr. 2019.
- [45] L.-W. Ko, Y. Chang, P.-L. Wu, Y.-C. Lu, C.-L. Yeh, and Y.-J. Chen, "Novel moisture retention sponge electrodes for developing a wireless EEG SSVEP-based BCI system," in *Proc. Int. Autom. Control Conf.* (CACS), Nov. 2018, pp. 1–5.
- [46] M. Kaya, M. K. Binli, E. Ozbay, H. Yanar, and Y. Mishchenko, "A large electroencephalographic motor imagery dataset for electroencephalographic brain computer interfaces," *Sci. Data*, vol. 5, no. 1, Dec. 2018, Art. no. 180211.
- [47] C.-R. Phang and L.-W. Ko, "Global cortical network distinguishes motor imagination of the left and right foot," *IEEE Access*, vol. 8, pp. 103734–103745, 2020.
- [48] C.-R. Phang and L.-W. Ko, "Intralobular and interlobular parietal functional network correlated to MI-BCI performance," *IEEE Trans. Neural Syst. Rehabil. Eng.*, vol. 28, no. 12, pp. 2671–2680, Dec. 2020.

- [49] L. Pion-Tonachini, K. Kreutz-Delgado, and S. Makeig, "ICLabel: An automated electroencephalographic independent component classifier, dataset, and website," *NeuroImage*, vol. 198, pp. 181–197, Sep. 2019.
- [50] C. Pehlevan and D. B. Chklovskii, "Optimization theory of Hebbian/anti-Hebbian networks for PCA and whitening," in *Proc. 53rd Annu. Allerton Conf. Commun.*, Control, Comput. (Allerton), Sep. 2015, pp. 1458–1465.
- [51] C. Yang, H. Zhang, S. Zhang, X. Han, S. Gao, and X. Gao, "The spatio-temporal equalization for evoked or event-related potential detection in multichannel EEG data," *IEEE Trans. Biomed. Eng.*, vol. 67, no. 8, pp. 2397–2414, Aug. 2020.
- [52] S. M. Shafiul Hasan, M. R. Siddiquee, R. Atri, R. Ramon, J. S. Marquez, and O. Bai, "Prediction of gait intention from pre-movement EEG signals: A feasibility study," *J. Neuroeng. Rehabil.*, vol. 17, no. 1, pp. 1–16, Dec. 2020.
- [53] K. A. Robbins, J. Touryan, T. Mullen, C. Kothe, and N. Bigdely-Shamlo, "How sensitive are EEG results to preprocessing methods: A benchmarking study," *IEEE Trans. Neural Syst. Rehabil. Eng.*, vol. 28, no. 5, pp. 1081–1090, May 2020.



Bo-Yu Tsai received the B.S. degree in biomedical engineering from National Cheng Kung University, Tainan, Taiwan, in 2018 and the master's degree in biomedical engineering from National Yang Ming Chiao Tung University (National Chiao Tung University), Hsinchu, Taiwan, in 2020.

He works as a System Engineer with ELAN Microelectronics Corporation, Hsinchu, where he is developing integrated circuits for touch sensor applications.



Sandeep Vara Sankar Diddi (Student Member, IEEE) received the bachelor's degree in electronics and communication engineering from Jawaharlal Nehru Technological University, Kakinada, India, and the master's degree in electronics and communication engineering from the National Institute of Technology, Rourkela, India, in 2012 and 2014, respectively. He is currently pursuing the Ph.D. degree with the Neural Engineering Laboratory, National Yang Ming Chiao Tung University (National Chiao Tung University), Hsinchu, Taiwan,

under the International Ph.D. Program in Interdisciplinary Neuroscience, University System of Taiwan (UST).

From 2015 to 2020, he served as an Assistant Professor with the Department of Electrical, Electronics and Communication Engineering, GITAM University, India. His primary research interests include brain-machine interface, complexity analysis, signal processing, machine learning, and neural networks.



Li-Wei (Leo) Ko (Member, IEEE) received the Ph.D. degree from the Institute of Electrical and Control Engineering, National Chiao Tung University (NCTU), Hsinchu, Taiwan, in 2007.

He is currently a Professor with the Institute of Bioinformatics and Systems Biology, Department of Electronics and Electrical Engineering, and the Institute of Electrical and Control Engineering, National Yang Ming Chiao Tung University (NYCU, former NCTU), Taiwan. His primary research interests include brain-computer interface, neural engineer-

ing, computational neuroscience, and smart healthcare, especially to develop the wearable EEG device for the prevention, early diagnosis, and treatment enhancement of neurological diseases in clinical studies.

Dr. Ko served as the Director for the Interdisciplinary Neuroscience Ph.D. Degree Program and an Associate Director for the Digital Medicine Center in NYCU. He is also the Affiliate Scholar with the Institute for Neural Computation, University of California, San Diego (UCSD). In the International Academic Service, he has been the Chair of the IEEE Computational Intelligence Society (CIS) Taipei Chapter since 2019. He also serves as the Associate Editors for the IEEE TRANSACTIONS ON NEURAL SYSTEMS AND REHABILITATION ENGINEERING, Archives of Gerontology and Geriatrics, International Journal of Fuzzy Systems, and Journal of Chinese Institute of Engineers.



Shuu-Jiun Wang received the M.D. degree from the School of Medicine, National Yang Ming Chiao Tung University (NYCU), Taipei, Taiwan, in 1988.

He is a practicing Neurologist and Chair Professor, Vice Dean with the School of Medicine, the Director with the Brain Research Center, NYCU, and the Director with the Neurological Institute, Taipei Veterans General Hospital (TVGH), Taipei He has been a Headache Specialist and started the Headache Clinic with TVGH since 1996. His research interests include clinical studies, epidemiol-

ogy and neuroimaging studies of headache medicine, chronic migraine, cluster headache, reversible cerebral vasoconstriction syndrome, and spontaneous intracranial hypotension. He has authored over 400 scientific articles.

Prof. Wang was the recipient of the Bruce S. Schoenberg's International Neuroepidemiology Award from the American Academy of Neurology in 1994, the Seymour Solomon Lecture Award from the American Headache Society in 2010, the G. Nappi Cluster Headache Award from the European Headache Society in 2016, and the MacDonald-Critchley Lecture Award by the Migraine Trust London in 2020. He was the Founding President of the Taiwan Headache Society from 2005 to 2011, the President of the Taiwan Neurological Society from 2017 to 2019, and the Asian Regional Consortium of Headache from 2019 to 2021. He serves as an Associate Editor for Cephalalgia and the Journal of Headache and Pain.



Chi-Yuan Chang (Student Member, IEEE) received the B.S. degree in mechanical engineering from National Taiwan University, Taipei City, Taiwan, in 2014. He is currently pursuing the Ph.D. degree in bioengineering from the University of California, San Diego, San Diego, CA, USA, while with the Swartz Center for Computational Neuroscience.

His research interests include, but not limit to, artifact removal for EEG signal, signal processing, brain-computer interfaces, and mental health assessment.



Tzyy-Ping Jung (Fellow, IEEE) received the B.S. degree in electronics engineering from National Chiao Tung University, Hsinchu, Taiwan, in 1984, and the M.S. and Ph.D. degrees in electrical engineering from Ohio State University, Columbus, OH, USA, in 1989 and 1993, respectively.

He is currently the Co-Director of the Center for Advanced Neurological Engineering with the Institute of Engineering in Medicine, University of California at San Diego (UCSD), La Jolla, CA, USA, where he is also an Associate Director of the

Swartz Center for Computational Neuroscience with the Institute for Neural Computation, and an Adjunct Professor of Bioengineering. In addition, he is an Adjunct Professor of Computer Science with National Yang Ming Chiao Tung University, an Adjunct Chair Professor of the College of Education, National Tsing Hua University, Hsinchu, Taiwan, an adjunct Professor of the Department of Computer Science and Information technology, National Cheng Kung University, Tainan, Taiwan, and an Adjunct Professor of the School of Precision Instrument and Opto-Electronic Engineering, Tianjin University, Tianjin, China. His research interests are in the areas of biomedical signal processing, cognitive neuroscience, machine learning, EEG, functional neuroimaging, and brain–computer interfaces and interactions.